Available online at www.sciencedirect.com
SCIENCE DIRECT®
International Journal of Heat and Fluid Flow 24 (2003) 147–156
International Journal of HEAT AND FLUID FLOW
www.elsevier.com/locate/ijhff

Reynolds averaged simulation of unsteady separated flow

G. Iaccarino [a], A. Ooi [b,*], P.A. Durbin [c], M. Behnia [d]

[a] Center for Turbulence Research, Stanford University, Stanford, CA 94305-3030, USA
[b] Department of Mechanical and Manufacturing Engineering, University of Melbourne, Melbourne 3010, Australia
[c] Department of Mechanical Engineering, Stanford University, Stanford, CA 94305-3030, USA
[d] School of Mechanical and Manufacturing Engineering, University of New South Wales, Sydney 2052, Australia

Received 22 March 2001; accepted 3 September 2002

Abstract

The accuracy of Reynolds averaged Navier–Stokes (RANS) turbulence models in predicting complex flows with separation is examined. The unsteady flow around square cylinder and over a wall-mounted cube are simulated and compared with experimental data. For the cube case, none of the previously published numerical predictions obtained by steady-state RANS produced a good match with experimental data. However, evidence exists that coherent vortex shedding occurs in this flow. Its presence demands unsteady RANS computation because the flow is not statistically stationary. The present study demonstrates that unsteady RANS does indeed predict periodic shedding, and leads to much better concurrence with available experimental data than has been achieved with steady computation.

1. Introduction

Recent advances in computing power have spurred interest in simulating time dependent, Reynolds averaged flows for problems ranging from noise prediction to fluid/structure interaction. When the flow is not statistically stationary, Reynolds averaging is not synonymous with time-averaging. Hence, a proper Reynolds averaged Navier–Stokes (RANS) simulation must be time dependent. This increases computational expense substantially, but it is demanded by a proper application of RANS methodology.

When the flow is periodic in time, an unsteady RANS simulation must be averaged over one period to compare to time-averaged data. The computational cost and the resolution requirements are mainly related to the vortical flow structures shed by the geometry and wall layers. Despite the time dependence, and large vortical structures, unsteady RANS is not a simulation of the turbulence, only of its statistics. Turbulence modeling plays a crucial role in establishing and correctly predicting the complex behavior of such flows. Indeed, the remarkable accomplishment of RANS models is their ability to directly predict the underlying statistics of a highly irregular, turbulent flow.

Unsteady RANS should not be confused with large Eddy simulation (LES): indeed, comparisons to LES will be made herein. The latter employs *spatial*, not *ensemble*, averaging. Averaging is over a scale sufficient to filter small eddies, not resolved by the particular grid being used, but the stochastic nature of turbulent solutions to the full Navier–Stokes is retained. Hence, Reynolds averaged statistics must be evaluated by accumulating a large enough sample size. In a temporally periodic flow, the samples must be at a fixed phase in order to obtain statistics of the turbulent portion of the velocity.

The mesh and time-step requirements of RANS and LES are quite different. LES resolves the eddies of the turbulence itself, whereas unsteady RANS models the turbulence and resolves only unsteady mean-flow structures. Consequently, LES typically requires much higher spatial and temporal resolution, and is more costly. LES also requires very long integration time to build an ensemble averaged solution. On the other hand, a few shedding periods are usually enough for an unsteady RANS computation to converge to its limit cycle.

* Corresponding author.
E-mail address: a.ooi@unimelb.edu.au (A. Ooi).

0142-727X/03/$ - see front matter © 2002 Elsevier Science Inc. All rights reserved.
doi:10.1016/S0142-727X(02)00210-2

A question arises over whether RANS can predict flows with gross unsteadiness. If the unsteadiness is deterministic, then unsteady RANS is suitable; for instance, if a frequency spectrum shows a spike at a shedding frequency, amidst a broadband background of turbulence, then unsteady RANS is warranted—indeed demanded.

In the present work, flow around a square cylinder and over a surface mounted cube are computed. These flows exhibit characteristics common to all flows past bluff obstacles, including separation and large scale unsteadiness. The square cylinder is a much-studied case in which a coherent vortex street forms in the wake. It is included here for comparison with the flow over a surface mounted cube.

A surface mounted, square cylinder would not produce a vortex street because the wall acts like a splitter plate to destroy the anti-symmetry. But evidence from experiment and LES is that a coherent component exists to the unsteady flow round a cube. Are the poor agreements between RANS and data in previous studies of this flow due to erroneously computing it as statistically stationary? Will unsteady RANS produce a periodic solution? If the answer to the latter is yes, then there is likely to be a better agreement with experimental data.

For quantitative validation, reliable experimental databases are available in the literature for both geometries (Hussein and Martinuzzi, 1996; Lyn et al., 1995). Vortical structures in the surface mounted cube flow are sketched in Fig. 1, taken from Hussein and Martinuzzi (1996): a strong horseshoe vortex and an arch-shaped vortex in the near wake were inferred from analysis of oil-flow patterns on the wind tunnel floor. This qualitative view suggests flow features that should be captured in a simulation.

LES of these flows have been carried out with considerable success (Shah, 1998). These test cases were selected for the 'Workshop on Large Eddy Simulation of Flows Past Bluff Bodies' (Rodi et al., 1997). In the workshop, several LES calculations were compared to data, showing good agreement. Steady-state RANS computations with different variations of the k–ϵ model were also presented: in general, unsatisfactory agreement with experimental data was obtained (see Rodi, 1997, 2002). This paper will show that the poor agreement was due to the assumption of statistical stationarity, not to the use of Reynolds averaged simulation.

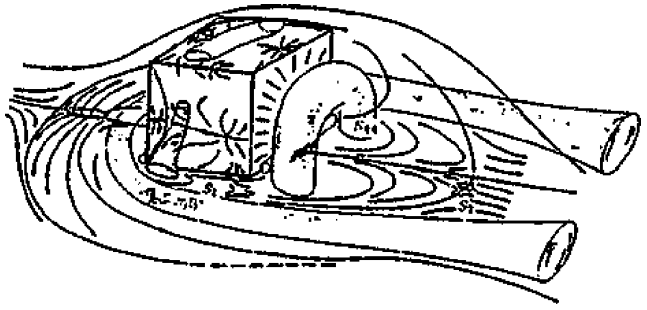

Fig. 1. Schematic representation of the main flow features of the cube, from Hussein and Martinuzzi (1996).

2. Numerical model

Two- and three-dimensional steady and unsteady RANS simulations were carried out using the v^2–f turbulence model (Durbin, 1995); an analysis of the effect of turbulence modeling is out of the scope of the present paper, but a very comprehensive study can be found in Breuer et al. (1996), Lakehal and Rodi (1997) and Lakehal and Thiele (2001).

A commercial computational fluid dynamics (CFD) code, FLUENT 5.5, was used to solve the equations of motion. The v^2–f model was implemented via user defined functions and was verified by comparison to computations with research codes (Iaccarino, 2001).

The spatial derivatives are discretized using a second order upwind scheme while the time integration employs a fully implicit second-order backward stencil (Barth and Jespersen, 1989). The SIMPLE algorithm is used for pressure–velocity coupling. The flow over the cylinder is two-dimensional, while full three-dimensional calculations are performed for flow over the surface mounted cube.

Initially, a very large time step was employed, producing a steady solution; note that both problems have an inherent geometrical symmetry and (provided that the grid is also symmetric) the flow field should remain symmetric: no vortex shedding is allowed. After the steady state is reached, a small unsymmetric perturbation in the velocity field is imposed to trigger the unsteadiness and time accurate simulation (with small timesteps) are carried out (Rogers and Kwak, 1990). The choice of the time step is based on an a priori estimate of the shedding period (based on experimental evidence); about 50 timesteps per period are necessary to obtain converged force coefficients (both in terms of averaged and r.m.s. values).

Coherent vortex shedding was obtained after several flow-through times ($\approx$3 for the square cylinder and $\approx$10 for the cube). A time-averaged solution was computed over a duration of four periodic cycles for both cases. In what follows, this is often referred to as the unsteady solution, dropping the qualification that it was subsequently time averaged for comparison to data.

The equations were solved on structured grids (12,000 and 500,000 cells for the square and the cube respectively), with a strong clustering close to the walls to capture the near-wall turbulent regions ($y^+ < 1$ at the first grid points away from all walls).

The flow conditions for the first test case correspond to the experiments by Lyn et al. (1995). The Reynolds number based on the inlet velocity (U_i), and the size of the square, h, is 22,000. The domain size is that recommended in Rodi et al. (1997), $20h \times 14h$ in the streamwise and spanwise directions, respectively; the square is located at $x = 5h$ from the inlet section. A small (2%) turbulence intensity is imposed at the inlet corresponding to the experimental values. The unsteady calculations are performed using a timestep $\tilde{\Delta}t = \Delta t U_i/h = 0.05$; the time averaged drag changed by less than 3% when the timestep was halved and less than 5% when it was doubled. The predicted results are also compared to similar unsteady RANS simulations performed by Bosch (1995) using a two-layer k–ϵ model with the Kato and Launder (1993) modification.

The flow conditions for the second test case correspond to the experiments by Hussein and Martinuzzi (1996); the Reynolds number based on the inlet bulk velocity, u_b, and the height of the cube, h, is 40,000. The domain size is the same as in Shah (1998): $20h \times 2h \times 6h$ in the streamwise, wall normal and spanwise directions, respectively. The cube is located at $x = 6h$ from the inlet. A fully developed channel flow solution is applied at the inlet, and solid walls are imposed in the spanwise direction, as in the experiment (the LES simulation by Shah (1998) employed a periodic condition in the span, which should cause some discrepancy to the experiment). As in the previous case a timestep $\tilde{\Delta}t = 0.05$ has been used, with similar results in terms of sensitivity of the force coefficients. For this case the RANS results reported in Rodi et al. (1997) are obtained using the same model mentioned before (k–ϵ model with the Kato and Launder modification) but only steady simulations were carried out; these results will be compared to the present findings.

3. Results and discussion

The flow around a square cylinder at the Reynolds number investigated presents coherent vortex shedding, with a periodically oscillating wake. The length of the recirculation region and the surface loads are of primary interest. A summary of the present simulations and several experimental data are reported in Table 1. As expected, the predictions obtained under steady-state assumptions are incorrect, with an extremely elongated recirculation bubble. Time accurate results, on the other hand, capture the size of the bubble, as well as the overall drag. This last result is also in good agreement with the LES and RANS results reported in the literature (Rodi et al., 1997). The intensity of the fluctuating loads is only in fair agreement with the experimental observation: the r.m.s. lift is overestimated whilst the r.m.s. drag is underestimated. The latter is of limited concern because it is small compared to the mean drag, and to the fluctuating lift. A possible explanation for the overprediction of r.m.s. lift can be found in the assumption of two-dimensional flow, which certainly will not hold away from the cylinder, where endwalls in the experiment exert an influence. It is worth noting that LES, which applies periodic endwall conditions, shows a better agreement with measurements of unsteady loads.

A qualitative picture of the vortex shedding behind the cylinder is presented in Fig. 2. Pressure isobars at four snapshots corresponding to a full period of wake oscillation are reported. Vortices are shed alternatively from the two sides of the square and then convected downstream; similar features are seen in Fig. 3, where streamlines are plotted. These figures will later be contrasted to results obtained for the surface mounted cube.

In addition, velocity profiles at four stations in the wake of the cylinder are reported in Fig. 4; the distribution on the centerline in Fig. 5. Very good agreement is obtained between the *unsteady* solution and the experimental measurements. The *steady* solution shows a recirculation bubble that is too long and thick.

Flow over a wall-mounted cube is visualized in Fig. 6. The left column contains streamlines computed of the time-averaged velocity field. The right column of Fig. 6 shows contours of streamwise velocity (u/u_b). In all calculations, an upstream recirculation bubble exists, together with primary and secondary recirculation regions downstream of the block.

Table 1
Results for the square cylinder

Contribution	Model	x_R/h	$\overline{C_d}$	$\widetilde{c_d}$	$\widetilde{c_l}$	St
Lyn et al., 1995	Experiments	1.38	2.1	–	–	0.132
Lee, 1975	Experiments	–	2.05	0.16–0.23	–	–
Vickery, 1966	Experiments	–	2.05	0.1–0.2	0.68–1.32	–
Rodi et al., 1997	LES[a]	1.32	2.2	0.14	1.01	0.13
Rodi et al., 1997	RANS[b]	1.25	2.004	–	–	0.143
Present RANS	Steady	4.81	1.71	–	–	–
Present RANS	Unsteady	1.45	2.22	0.056	1.83	0.141

x_R/h: recirculation length, $\overline{C_d}$: time averaged drag coefficient, $\widetilde{c_d}$ and $\widetilde{c_l}$: root mean square of drag and lift coefficient, St: Strouhal number.
[a] LES by Porquie, Breuer and Rodi referred to as UKAHY1 in Rodi et al. (1997).
[b] RANS by Bosch using a two-layer k–ϵ model reported in Rodi et al. (1997).

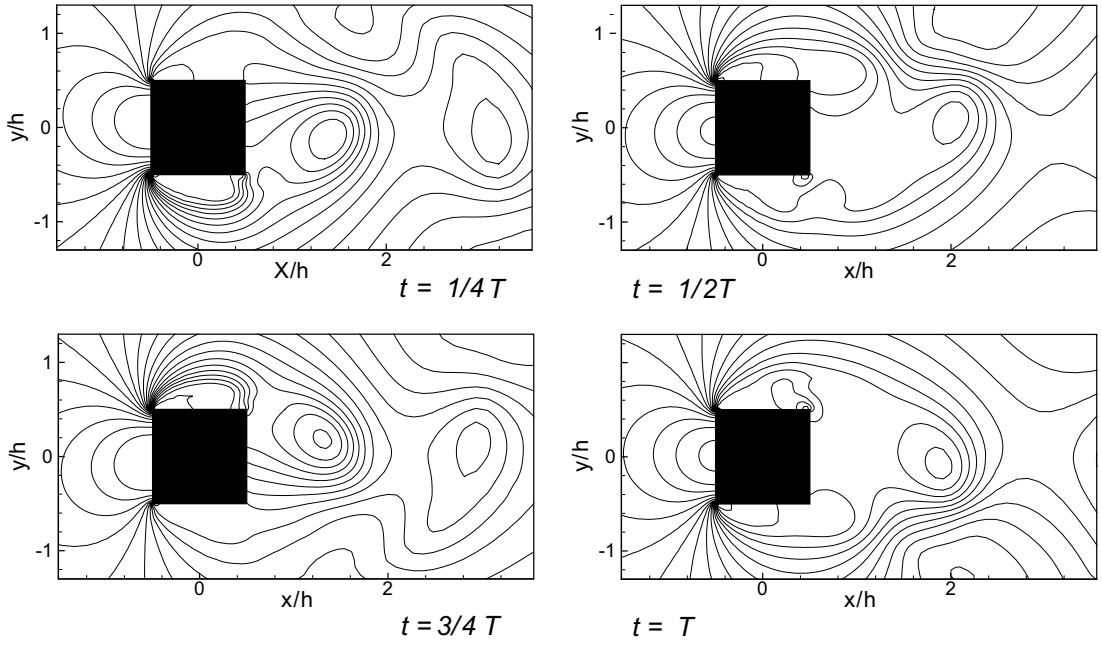

Fig. 2. Time history of the pressure distribution in the wake of the square cylinder.

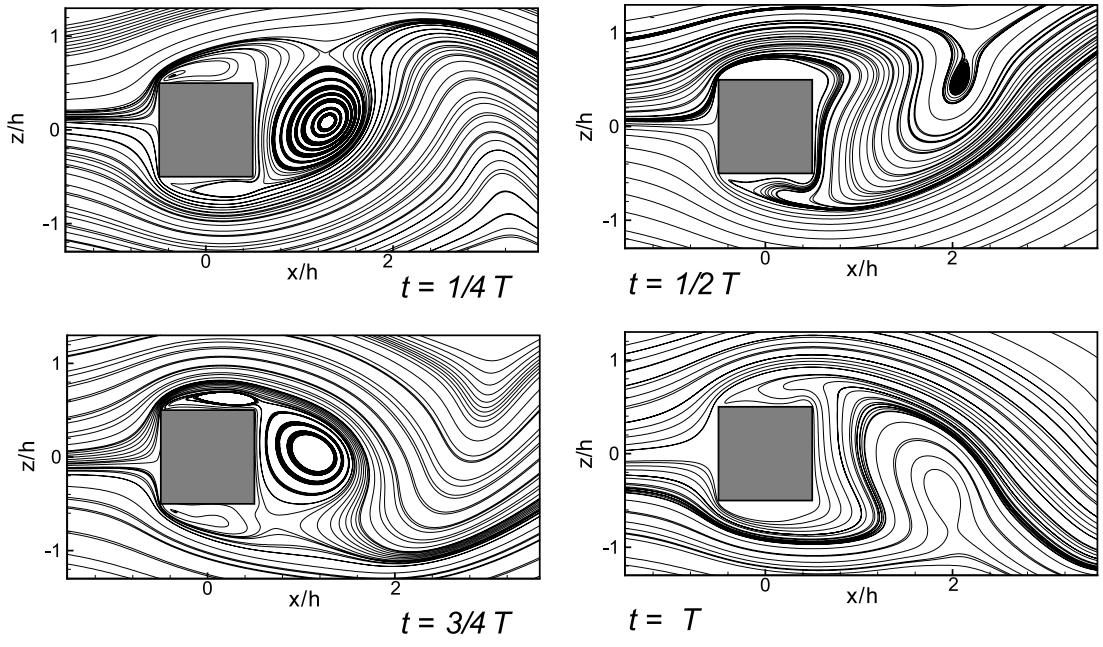

Fig. 3. Time history of the streamlines in the wake of the square cylinder.

The streamlines in Fig. 6 suggest that the vortex cores in all calculations are in the same locations and that broad features of the flow are in remarkable agreement. However, it is evident that the steady solution yields a recirculation area in the wake of the cube that is too large—although the flow pattern is fairly good elsewhere. Table 2 is a summary of the length of the downstream and upstream recirculation bubbles from the experimental data, and from previous numerical studies by Rodi et al. (1997) and Shah (1998). The most critical length is that of the large recirculation zone behind the body, denoted x_{R1}; the other eddies are much smaller.

For this primary downstream bubble, the experimental data and LES indicate a separation length of $\approx 1.6h$. Steady-state RANS solutions overpredict the extent by more than 100% ($3.3h$). On the other hand, the unsteady RANS solution predicts a reattachment length

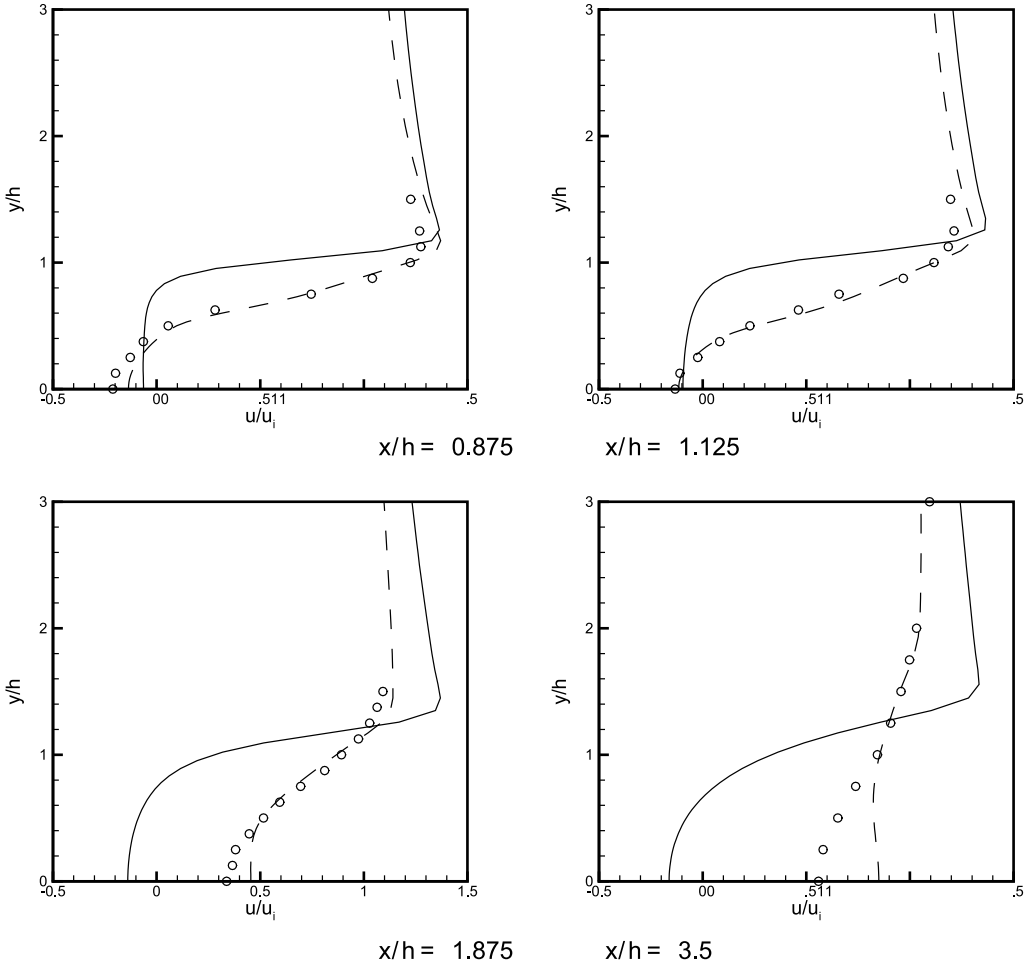

Fig. 4. Streamwise velocity profiles in the wake of the cylinder. (—) steady solution; (– – –) unsteady solution; (○) experiments. $y/h = 0$ corresponds to the wake centerline.

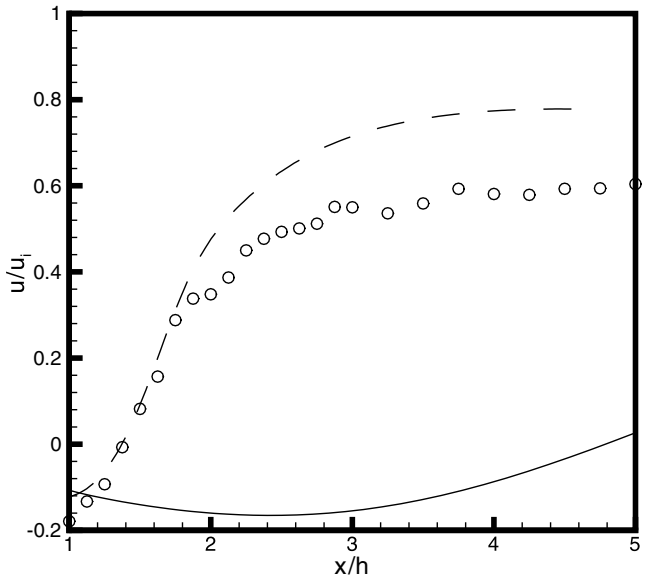

Fig. 5. Streamwise velocity profiles in the wake centerline of the cylinder. (—) steady solution; (– – –) unsteady solution; (○) experiments.

of $\approx 1.9h$, in much better agreement with the measurements. The streamline and velocity contour plots (Fig. 6) show the global nature of the improvement.

Flow visualizations of the unsteady RANS solution are next reported. In Fig. 7, the horseshoe vortex is represented via the λ_2 vortex-detection criterion of Jeong and Hussain (1995) while the arch vortex in the wake is visualized using an isosurface of the pressure. The λ_2 detection method did not reveal the arch vortex; a combination of pressure and velocity gradient criteria were required to reveal both the horseshoe and arch vortical structures. These are the same features seen in Fig. 1. The vortical structure for both the experiment and the RANS were extracted from the time-averaged flow.

The time evolution of the pressure distribution on the wind tunnel floor over one period is reported in Fig. 8: the flow is indeed periodic, showing a side-to-side oscillation. Comparison between Figs. 8 and 2 shows a distinction between the two flows. Eddies are observed to convect downstream and exit the region, four diameters beyond the square cylinder, included in Fig. 2. By

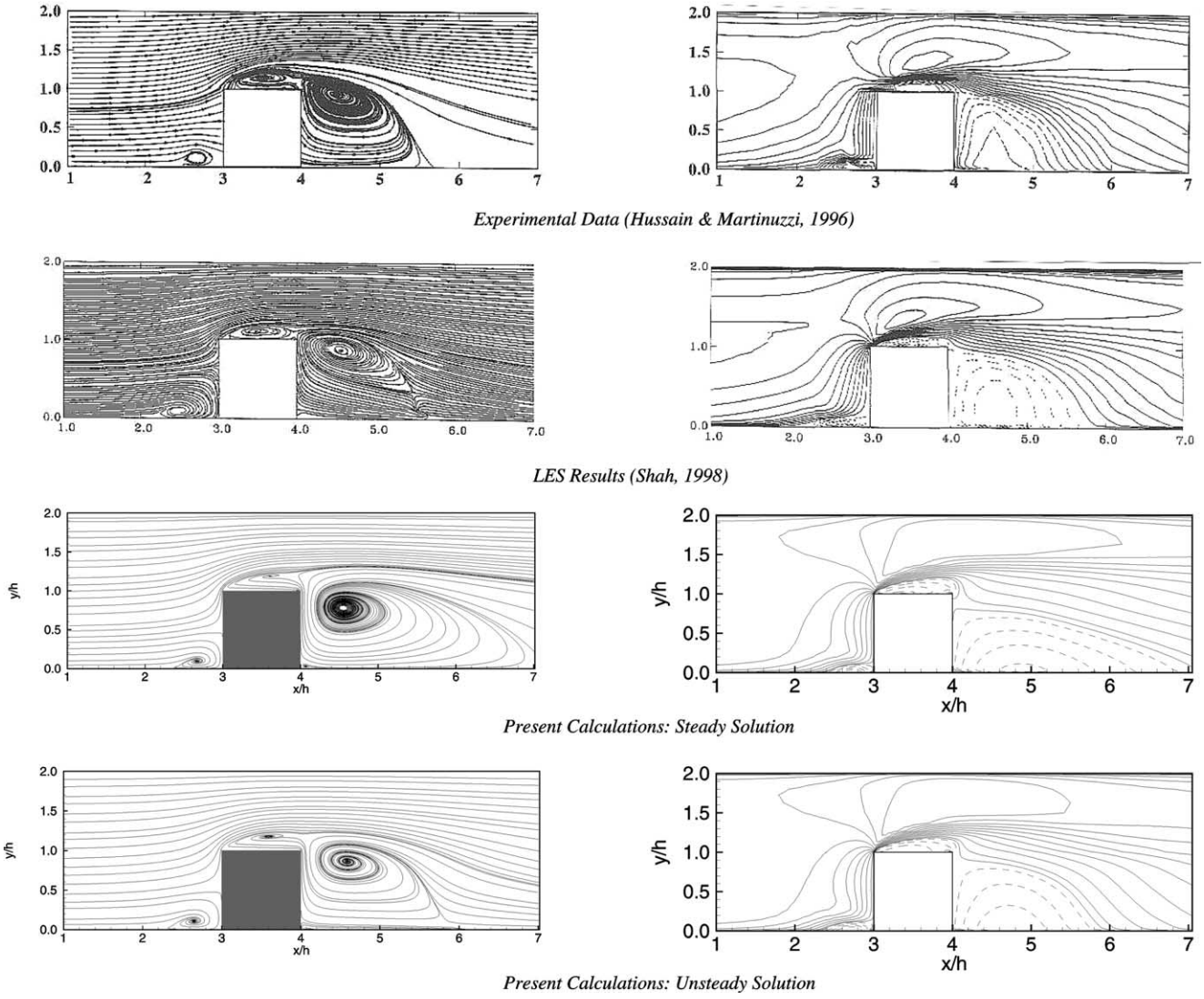

Fig. 6. Streamlines (left column) and streamwise velocity (right column) on the symmetry plane. Dashed lines indicate negative velocity.

Table 2
Length of recirculation bubbles in the flow over a surface mounted cube

Contribution	Model	x_F/h	x_{R_1}/h	x_{R_2}/h
Martinuzzi and Tropea, 1993	Experiments	1.040	1.612	–
Rodi et al., 1997	LES[a]	0.998	1.432	0.134
Rodi et al., 1997	RANS[b]	0.950	2.731	0.252
Shah, 1998	LES	1.080	1.690	0.160
Present RANS	Steady	0.640	3.315	0.310
Present RANS	Unsteady	0.732	1.876	0.204

x_F/h: upstream separation length; x_{R_1}/h and x_{R_2}/h: downstream primary and secondary recirculation length.
[a] LES by Porquie, Breuer and Rodi referred to as UKAHY4 in Rodi et al. (1997).
[b] RANS by Breuer using a two-layer k–ϵ model reported in Rodi et al. (1997).

four diameters downstream, Fig. 8 shows negligible eddying behind the cube, with an almost complete pressure recovery. Oscillatory unsteadiness is confined to the immediate rear of the cube.

At the outset of this study, it was far from obvious that a RANS simulation would predict periodic unsteadiness behind the cube, especially with an eddy viscosity formulation. Eddy viscosity represents the ensemble average effect of random convection mathematically as a diffusive process. Even if coherent unsteadiness *should* be present, it was not certain that the model would admit it.

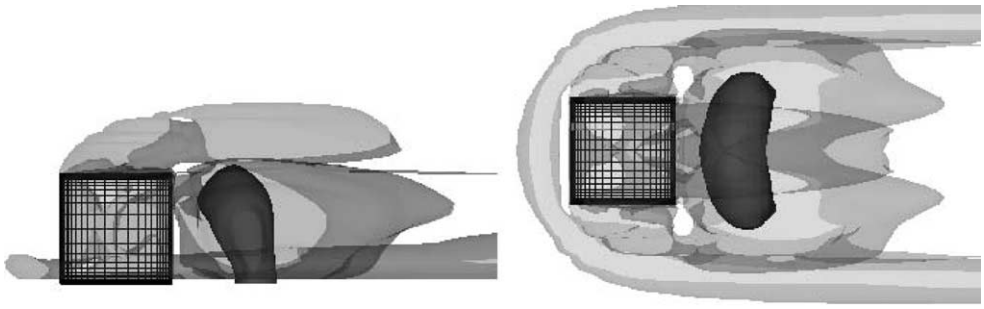

Fig. 7. Side and top view of the vortical structure (cf. to Fig. 1). The horseshoe vortex is represented using the λ_2 criterion (Jeong and Hussain, 1995), while the arch-vortex is visualized using an isobar surface.

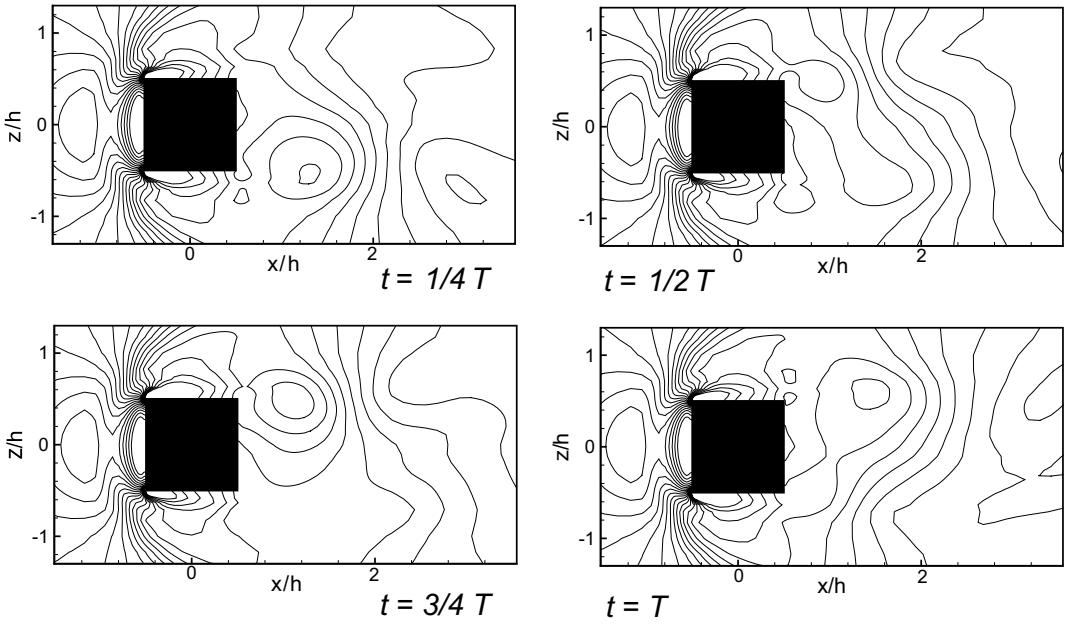

Fig. 8. Time history of the pressure distribution on the floor.

The arch vortex appears to be the origin of unsteadiness. Vorticity shed from the side of the cube induces an oscillatory yaw of the arch vortex. One leg becomes stronger by acquiring vorticity from the detached boundary layer on that side of the cube. As that leg moves downstream, the leg on the opposite side strengthens. Thus, the shedding develops a side-to-side oscillation. But this is not analogous to a vonKarman vortex street: after detaching, the arch vortex becomes nearly symmetric as shown in Fig. 7.

Another view is presented by Fig. 9, where the skin friction lines on the wind tunnel floor are reported. This figure can be contrasted to Fig. 3: the square cylinder sheds distinct, well-separated vortices of opposite sign; the cube sheds a closely spaced pair. A rather intriguing pattern of foci, saddles and lines of attachment is seen in Fig. 9. The foci reflect the arch vortex, the attachment lines lie under the horseshoe vortex. At $t = 1/4T$ and T one focus appears to be merged with one attachment line. This seems to reflect merging of the arch vortex into an extended horseshoe vortex, as is seen in Fig. 7. As reference, the experimental oil-film flow visualisation is reported in Martinuzzi and Tropea (1993). A comparison between the friction lines obtained in a steady-state calculation, the time-averaged calculation and experimental data of Martinuzzi and Tropea (1993) is shown in Fig. 10. The patterns are similar but the extent of the primary recirculation behind the wake is sensibly larger in the data of the steady calculation than the time-averaged data from the unsteady calculation. It is clear that time-averaged data from the unsteady calculation provide a better match with the experimental data.

The surface pressure contours of Fig. 8 are its oscillatory footprint. Unsteadiness is primarily seen in the immediate lee of the cube. The shedding corresponds to a Strouhal number of 0.17 (experimental value 0.145).

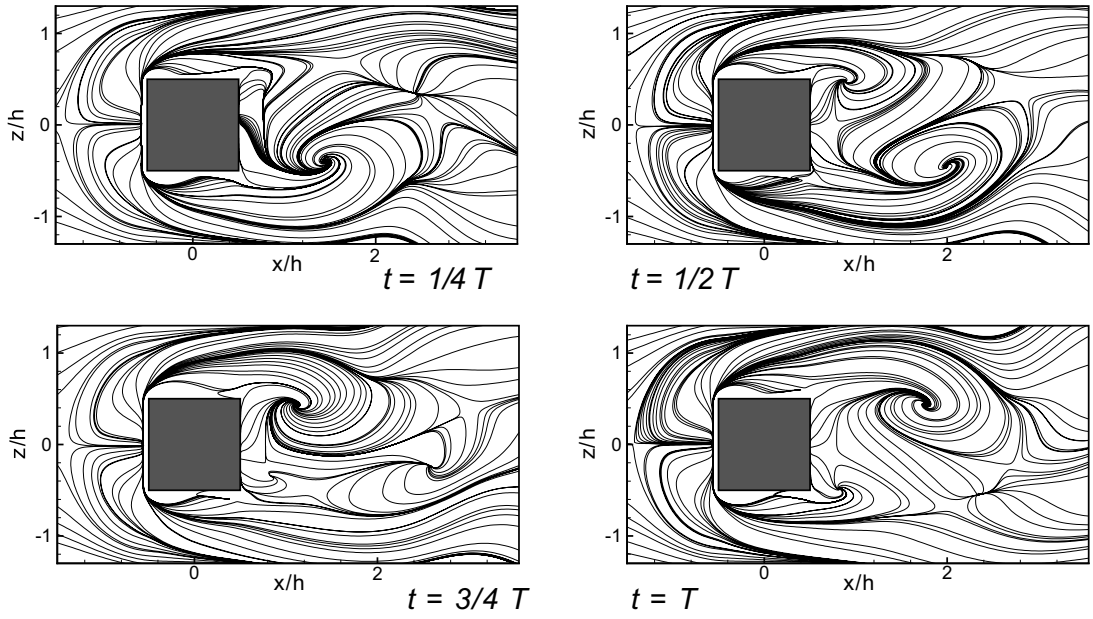

Fig. 9. Time history of the skin-friction lines on the floor.

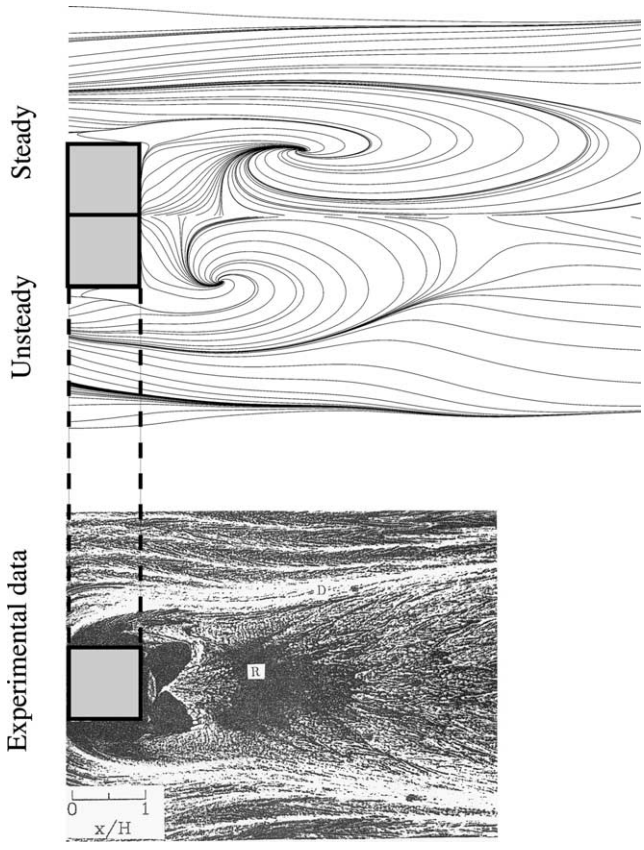

Fig. 10. Steady (top), time-averaged (middle) and experimental (bottom) skin-friction lines on the floor. The experimental data is taken from Fig. 6(b) of Martinuzzi and Tropea (1993).

No vortex shedding is observed from the boundary on the roof of the cube, and unsteadiness of the horseshoe vortex, wrapped around the base of the cube (Fig. 7), is weak.

A quantitative comparison between the computations and data is reported in Fig. 11. Streamwise velocity profiles at four stations on the symmetry plane are shown. The agreement between the experimental data and the unsteady solution is satisfactory. The main discrepancy is due to the inadequate prediction of the high-speed flow between the cube and the wind tunnel roof. The over prediction of the velocity in that region may be due to incorrect capturing of the separated boundary layer on the cube roof. As expected, the steady solution significantly over predicts the strength of the recirculation velocity in the wake; this conclusion is also confirmed by the steady RANS results reported in Lakehal and Rodi (1997) using several different turbulence models.

4. Discussion

This paper has shown that unsteady RANS provides good quantitative and qualitative agreement with experimental data when the flow is not statistically stationary. The present simulation of the three-dimensional vortex shedding behind a surface mounted cube is one of the most ambitions computations of this ilk, to date. It serves to highlight the need to apply RANS models in a manner that is consistent with the definition of the Reynolds (or ensemble) average, notwithstanding the increased computational cost. Steady computations produce an erroneously long wake because they omit an important component of the averaged flow field, the periodic vortex shedding.

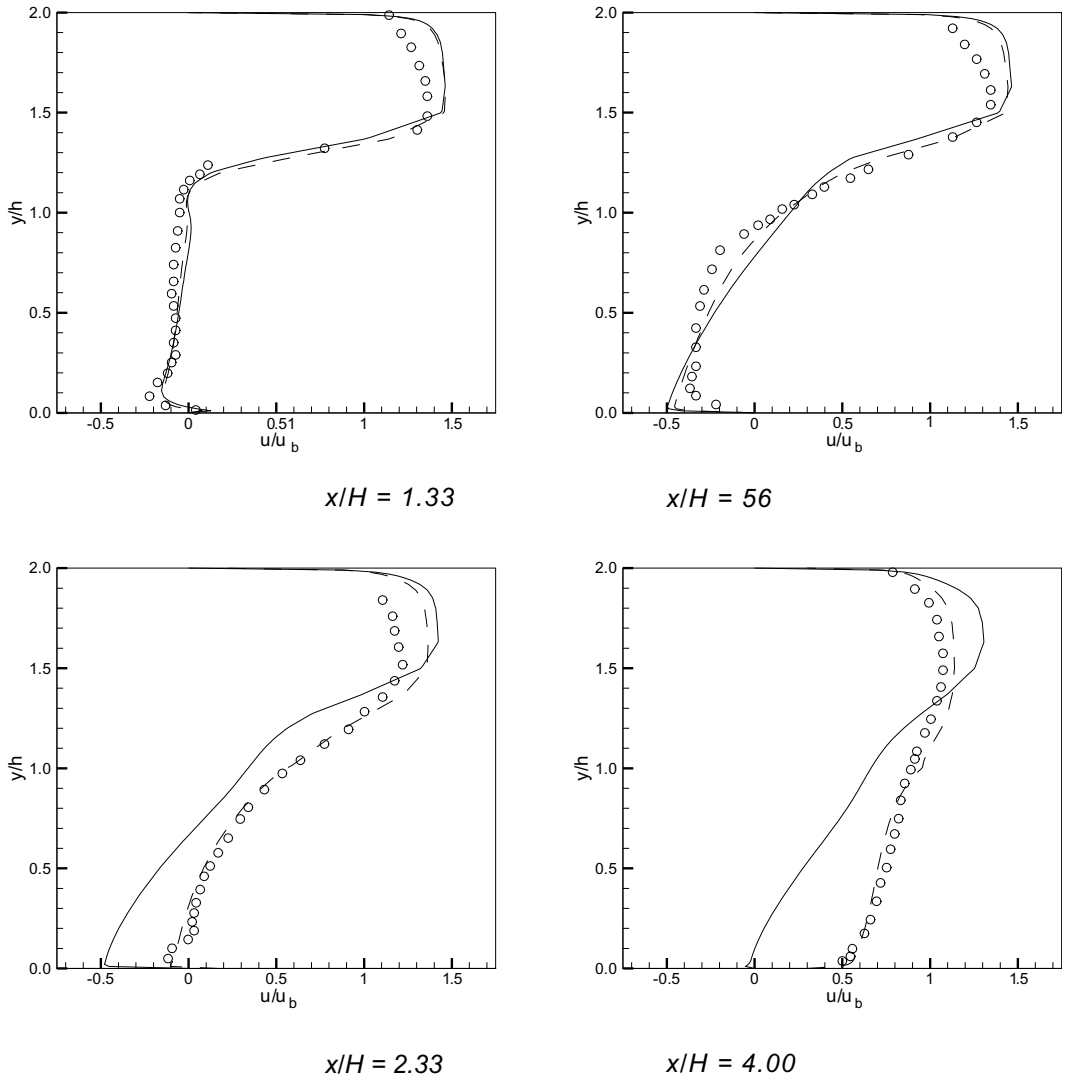

Fig. 11. Streamwise velocity profiles in the symmetry plane. (—) steady solution; (– – –) unsteady solution; (O) experiments. $y/h = 0$ corresponds to the wind-tunnel floor.

The unsteady computations reproduced essential physics of three-dimensional, massively separated flows: the horseshoe vortex and the arch-shaped vortex in the near wake, inferred by analysis of experimental oil-flow patterns, were visualized by means of two vortex-detection criteria. The two side walls of the surface mounted cube are the origin of the periodically unsteady, arch vortex. A fully resolved, three-dimensional computation is required to simulate it.

References

Barth, T.J., Jespersen, D., 1989. The Design and Application of Upwind Schemes on Unstructured Meshes, AIAA Paper 89-0366.

Bosch, G., 1995. Experimental and Theoretical Study of the Unsteady Flow Around a Cylindrical Structure. Ph.D. Thesis, University of Karlsruhe.

Breuer, M., Lakehal, D., Rodi, W., 1996. Flow Around a Surface Mounted Cubical Obstacle: Comparison of LES and RANS-Results, IMACS-COST Conference on CFD, Three-Dimensional Complex Flows, Lausanne, Switzerland, 13–15 September.

Durbin, P.A., 1995. Separated flow computations with the k–ϵ–v^2 model. AIAA J. 33, 659–664.

Hussein, H.J., Martinuzzi, R.J., 1996. Energy balance for the turbulent flow around a surface mounted cube placed in a channel. Phys. Fluids 8, 764–780.

Iaccarino, G., 2001. Predictions of a turbulent separated flow using commercial CFD codes. J. Fluids Eng. 123, 1–10.

Jeong, J., Hussain, F., 1995. On the identification of a vortex. J. Fluid Mech. 285, 69–94.

Kato, M., Launder, B.E., 1993. The modelling of turbulent flow around stationary and vibrating square cylinders. Proceedings of the 9th Symposium on Turbulent Shear Flows Kyoto. pp. 10.4.1–10.4.6.

Lakehal, D., Rodi, W., 1997. Calculation of the flow past a surface-mounted cube with two-layer turbulence models. J. Wind Eng. 67, 65–78.

Lakehal, D., Thiele, F., 2001. Sensitivity of turbulent shedding flows to non-linear stress–strain relations and Reynolds stress models. Comp. Fluids 30, 1–35.

Lee, B.E., 1975. The effect of turbulence on the surface pressure field of a square prism. J. Fluid Mech. 69, 263–289.

Lyn, D.A., Einav, S., Rodi, W., Park, J.H., 1995. A laser-Doppler velocimetry study of ensemble averaged characteristics of the turbulent near wake of a square cylinder. J. Fluid Mech. 304, 205–232.

Martinuzzi, R., Tropea, C., 1993. The flow around surface mounted, prismatic obstacles placed in a fully developed channel flow. Trans. ASME J. Fluids Eng. 115, 85–93.

Rodi, W., 1997. Comparison of LES and RANS calculations of the flow around bluff bodies. J. Wind Eng. Ind. Aerodyn. 69–71, 55–75.

Rodi, W., 2002. Closure strategies for turbulent and transitional flows. In: Launder, B.E., Sandham, N.D. (Eds.), Large-Eddy Simulations of the Flow Past Bluff Bodies. Cambridge University Press, pp. 361–391.

Rodi, W., Ferziger, J.H., Breuer, M., Pourquie, M., 1997. Status of large eddy simulation: result of a workshop. J. Fluids Eng. 119, 248–262.

Rogers, S.E., Kwak, D., 1990. An upwind differencing scheme for the time-accurate incompressible Navier–Stokes equations. AIAA J. 28, 253–262.

Shah, K.B., 1998. Large Eddy Simulation of the Flow Past a Cubic Obstacle. Ph.D. Thesis.

Vickery, B.J., 1966. Fluctuating lift and drag on a long square cylinder of square cross section in a smooth and turbulent stream. J. Fluid Mech. 25, 481–503.